Programme Area: Carbon Capture and Storage

Project: Benchmark Refresh

Title: CO2 separation using a rotary wheel adsorber

Abstract:

This report presents the results of an independent assessment (by University of Edinburgh, UoE) of the likely achievable separation performance from a rotary wheel adsorber using carbon monolith adsorbents. UoE selected what it considered the best available grade of carbon, measured adsorption isotherms for N2 and CO2 and modelled the performance of a rotary adsorber for two alternative cycles. The simulation results showed that 90% recovery and 97% purity could be achieved.

Context:

This project refreshed and extended techno-economic studies of current generation (benchmark) CO2 capture technologies for gas fired power stations and provided comparable information on one or more next generation technologies. It produced a new benchmark incorporating exhaust gas recycle and provided robust, independent and directly comparable technology assessments of specific technologies being considered for further demonstration.

CO_2 separation using a rotary wheel adsorber. A report prepared for the ETI (12/03/2015).

Enzo Mangano and Stefano Brandani

School of Engineering, The University of Edinburgh

The King's Buildings, Edinburgh, EH9 3JL

In this document a detailed study on the performance of CO_2 separation using a rotary wheel adsorber is reported. This report should be read in conjunction with the presentation given on 23/02/2015. The study focuses on different ranges of conditions and process configurations which meet the pre-set requirement in CO_2 purity of 97% and recovery of 90% using a carbon monolith. The following sections describe the details of the different cases analysed and discuss the results obtained.

Adsorbent Characterisation

The adsorbent selected for the separation is a carbon monolith. The geometry is assumed to be the same as MAST monoliths with square channels (data from Agueda et al. 2011). The parameters for the adsorption isotherm of both CO_2 and N_2 have been measured at different temperatures using a Quantachrome Autosorb iQ volumetric apparatus on a commercial sample of activated carbon (SRD 10 091 - Chemviron Carbon, Calgon). The experiments were carried out at 5, 25, and 45 °C using 0.9984 g of adsorbent (2 mm particle size). Figure 1 shows the isotherms for both CO_2 and N_2 and the Dual Site Langmuir (DSL) model used to regress the data. The DSL isotherm is given by eq. 1, while the parameters obtained from the fitting of the experimental data are listed in Table 1.

$$q^i = \frac{q^i_{s1} b^i_1 P}{1+b^i_1 P} + \frac{q^i_{s2} b^i_2 P}{1+b^i_2 P} \quad (1)$$

where:

$$b^i_k = b^i_{0k} \exp\left(-\frac{\Delta H^i_k}{RT}\right) \quad (2)$$

Table 1. Parameters of the Dual Site Langmuir Isotherm

DSL parameters	CO_2	N_2
qs_1, mol/kg	0.458	0.458
qs_2, mol/kg	3.292	3.292
b_{01}, 1/bar	4.737×10^{-6}	1.276×10^{-5}
b_{02}, 1/bar	4.092×10^{-6}	2.66×10^{-5}
ΔH_1, kJ/mol	39.48	23.47
ΔH_2, kJ/mol	30.09	18.24

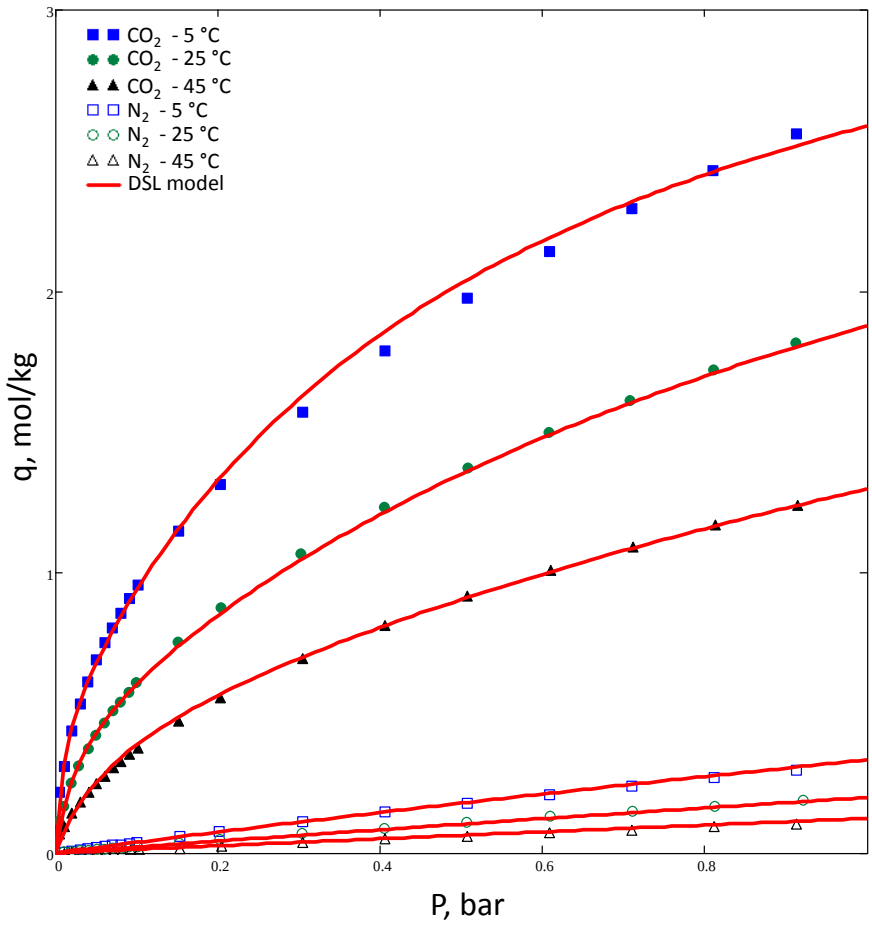

Figure 1: Experimental equilibrium isotherms for CO_2 and N_2 on AC SRD 10 091 with the fitted curves of the Dual Site Langmuir model (Table 1).

The density of the adsorbent was measured at 25 °C on a Quantachrome UltraPyc 1200e He pycnometer. In order to estimate the heat capacity of the solid, calorimetric experiments in the range of 20 – 120 °C were also performed on a Setaram Sensys Evo TG/DSC system. Table 2 summarises the geometrical data of the monoliths (Agueda et al., 2011) along with the experimental data on the representative activated carbon adsorbent.

Table 2. Geometrical parameters of the monoliths

	High density	Low density
Density, mol/kg	1930	1930
Cp, J/(kg K)	995	995
ND, cell/cm^2	90.7	46.3
a (external dimension), m	1.05×10^{-3}	1.47×10^{-3}
b (internal dimension), m	6.965×10^{-4}	9.748×10^{-4}
w (half thickness), m	1.768×10^{-4}	2.474×10^{-4}
w_c (corrected half thickness), m	2.065×10^{-4}	2.89×10^{-4}
Length, m	1	1

CySim Simulations

The simulations were carried out using CySim, the adsorption cycle simulator developed at the University of Edinburgh. The system was assumed to be adiabatic (i.e. no heat losses to the environment) and the column was made only of the adsorbing monolith. Given that the main task was to determine the potential of the process configuration the assumption of fast mass transfer kinetics was made. In this case the axial dispersion is primarily due to numerical dispersion. The differential heat, mass and momentum balance equations where discretised using finite volume techniques. Different tests with different spatial grid points were carried out. As expected, by increasing the number of grid points a sharper concentration front is generated, but the corresponding simulation time increases significantly. It was decided to use 20 grid points since with this choice the numerical dispersion is acceptable and less than the corresponding dispersion due to mass transfer kinetics in similar monoliths (Brandani et al., 2004). The monolith is assumed to be ideal, ie each channel has the same size and gas flowrate, thus allowing the simulations to be carried out for a single channel (Ahn and Brandani, 2005a) with appropriately set boundary conditions. The pressure drop is estimated from the correlations for square channels given by Cornish (1928).

The inlet stream is assumed to contain only N_2 and CO_2 at atmospheric pressure and steam is used for the regeneration of the adsorbent. The length of the monolith is set to 1 m, since this is close to the characteristic length of the active section in rotary wheel heat regenerators, such as those produced by Howden. In an adsorption process, the cycle time can be adjusted once the length is set. If a shorter monolith is used, the cycle time would be reduced almost proportionately maintaining the concentration fronts inside the adsorber and the purity and recovery would remain unaffected up to the point where the mass transfer zone becomes the same length as the adsorber.

For this study we used process configurations already developed as part of the AMPGas project. Figure 2 shows the different main configurations used. The simplest one is the one in which the wheel is divided in two sectors, one for the adsorption step and one for the desorption step. In the second main configuration the wheel is divided in three sectors: adsorption, purge and cooling.

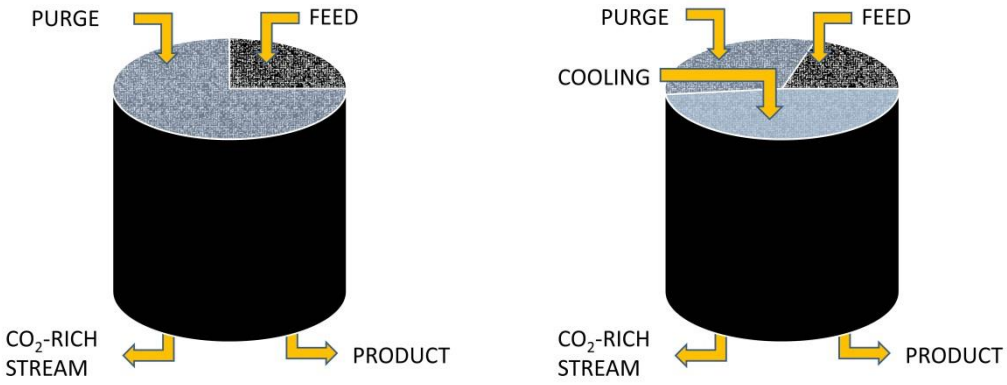

Figure 2: Configuration with adsorption-desorption step (left); Configuration with adsorption-desorption-cooling step (right).

Both configurations can be improved by adding a vent line at the outlet stream. In this way for a fraction of the cycle, the N_2 rich initial desorption flow is diverted in a separate stream improving the resulting CO_2 purity.

The flowrates and the cycle times were selected in order to allow the adsorption front to reach the outlet while keeping the pressure drop below the lower limit suggested (5 kPa). The purge step was carried out using steam at 125 °C (and in one case at 145 °C); it was assumed that the steam was not adsorbing in the monolith and the operating conditions were chosen in order to avoid condensation inside the bed (i.e final outlet temperature above 100 °C). For all the configurations the CO_2 composition in the feed stream was 10% vol. in N_2; as a comparison, one case with a feed CO_2 concentration of 4% was also considered (Table 8).

Configuration 1

All the simulations reported in these sections are carried out using steam at 125 °C and the high density monolith which will yield a higher process performance. Case 1 represents the simple adsorption/desorption configuration, while Case 2 refers to the case in which the vent line is implemented.

Table 3: Cycle parameters for Case 1 & 2.

Parameters	**Case 1**	**Case 2a**	**Case 2b**
Cycle time, s	70	70	70
Adsorption time, s	28	28	28
F_{feed}, $\frac{m^3/s}{m^2_{mon}}$	0.711	0.711	0.636
F_{purge}, $\frac{m^3/s}{m^2_{mon}}$	2.1	2.1	1.8
Max. Pressure drop, kPa	1.7 (ads) 4.25 (purge)	1.7 (ads) 4.25 (purge)	1.22 (ads) 3.39 (purge)
Max velocity, m/s	1.9 (ads) 5.14 (purge)	1.9 (ads) 5.14 (purge)	1.3 (ads) 4.9 (purge)
Venting time, s	–	0.865	1.01
Vol_{vent}, m^3/kg CO_2 captured	–	0.49	0.68
Steam required, kg of steam/kg CO_2 captured	10.23	11.28	9.81
CO_2 Recovery	90	81.6	90
CO_2 Purity	57.5	97	97

Table 3 reports the summary of the cycle parameters for Cases 1 and 2. The flowrates are reported as m^3/s of gas per m^2 of surface of monolith, assuming a cell density of 90.7 cells/cm^2, as reported in Table 2. The table also includes an evaluation of the steam required for each case. This is calculated as:

$$Steam\ required\ \left[\frac{kg}{kgCO_{2\ capture}}\right] = \frac{F^{in}_{STeam}}{F^{in}_{CO_2} \times Recovery}$$

Case 1 was used to gauge the conditions that would meet the constraint of 90% recovery, with the cyclic steady state temperature oscillating around approximately 106 °C. By introducing a short vent step, Case 2a, it is possible to flush out most of the N_2 and achieve 97% purity maintaining the same inlet flowrate (ie roughly the same unit productivity as in Case 1). From this point, by reducing the inlet specific flowrate during adsorption and slightly adjusting the vent step, Case 2b, it is possible to achieve both 90% recovery and 97% purity. Case 2b has a lower productivity and requires proportionately almost 9 kg of steam/kg of CO_2 captured.

Configuration 2

As mentioned above this configuration has a cooling step between the purge and the adsorption step. This is performed using N_2 at 10 °C, but in practice any inert gas would yield a similar result. Similarly to the cases above, a variant to the base configuration is considered with a vent line added to improve the CO_2 purity (case 4a,4b).

Table 4: Cycle parameters for Case 3 & 4 with lower pressure drop.

Parameters	**Case 3**	**Case 4a**	**Case 4b**
Cycle time, s	1430	1430	1430
Adsorption time, s	72.2	72.2	72.2
F_{feed}, $\frac{m^3/s}{m^2_{mon}}$	2.28	2.28	2.21
F_{purge}, $\frac{m^3/s}{m^2_{mon}}$	2.1	2.1	2.1
F_{N2}, $\frac{m^3/s}{m^2_{mon}}$	1.45	1.45	1.45
Max. Pressure drop, kPa	3.9 (ads) 4.18(cooling)	3.9 (ads) 4.18(cooling)	3.6 (ads) 4.18(cooling)
Max velocity, m/s	5.3 (ads) 4.6(cooling)	5.3 (ads) 4.6(cooling)	5.1 (ads) 4.76(cooling)
Vent time, s	–	1.51	1.51
Vol_{vent}, m^3/kg CO_2 captured		0.167	0.168
Heat duty, MJ/kg CO_2 captured	4.96	4.97	4.98
Steam required, kg of steam/kg CO_2 captured	3.19	3.29	3.29
CO_2 Recovery	90	87.4	90
CO_2 Purity	79.9	97	97

Table 4 reports the summary of cases studied. Here the heat from the steam is needed to desorb the CO_2 and reheat the solid bed.

With the cooling step, the increase in working capacity and the increase in selectivity at the lower adsorption temperature lead to a decrease in the ratio of steam to CO_2 captured, which is now around 3.

Figure 3 shows the concentration profile along the column for case 3. Figure 4 shows the breakthrough at the end of the column (length = 1 m) in terms of gas phase mole fractions for CO_2, N_2 and H_2O.

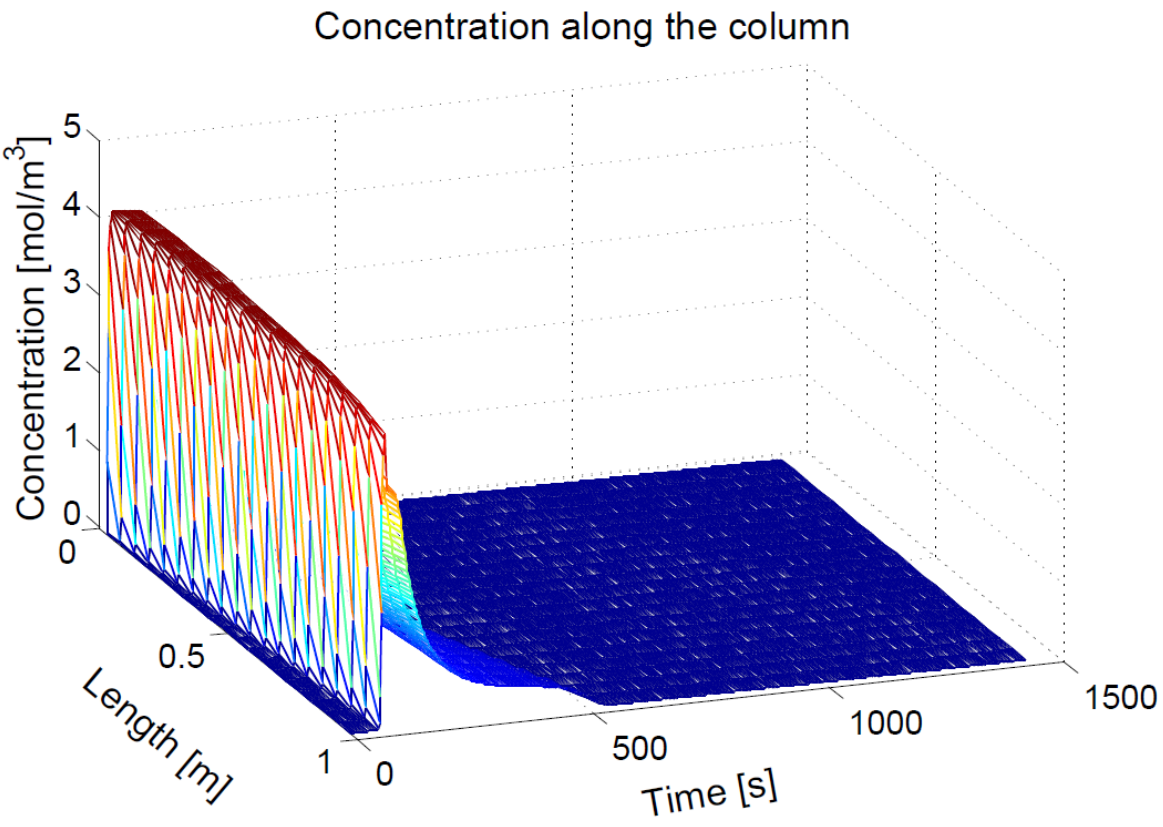

Figure 3: CO_2 concentration profile along the column for the steady state cycle for the Case 3 configuration.

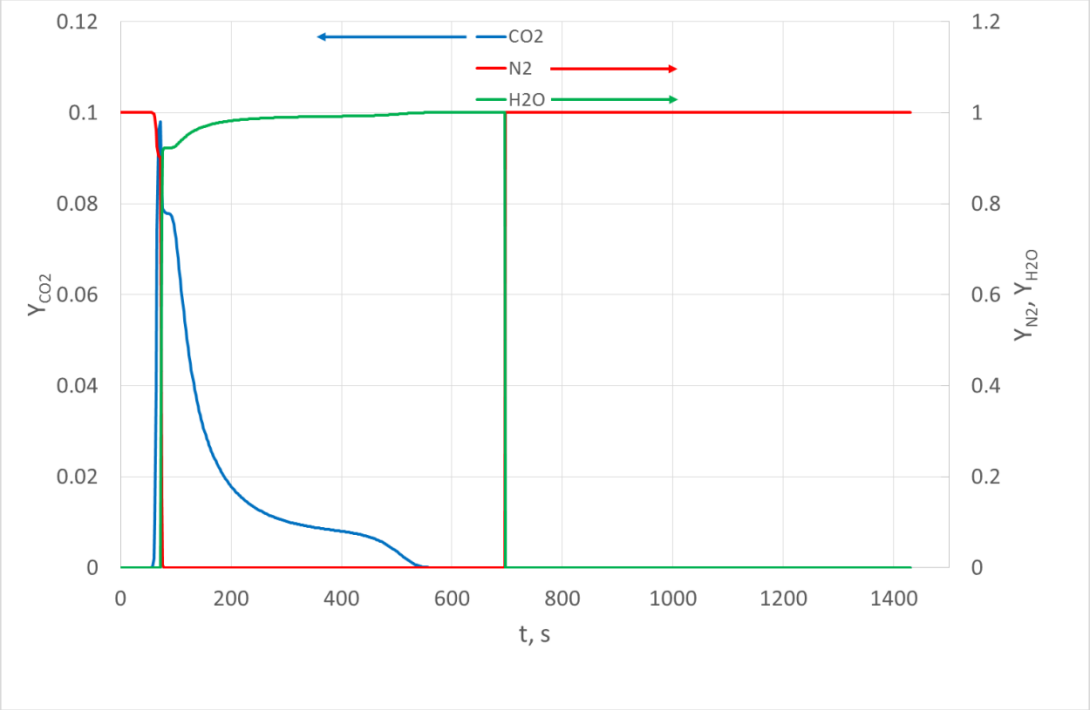

Figure 4: Breakthrough profile at the end of the column (profile at Length = 1m), as gas phase mole fractions during the various steps of the process for the system at cyclic steady state.

To allow a more accurate comparison with other processes, the table includes also an estimate of the heat duty. This is calculated applying an enthalpy balance between the inlet and the outlet flow during the purge step. Assuming the inlet steam temperature as the reference temperature, the enthalpy can be obtained as:

$$H_{inlet} = F_{steam} t_{ads} \int_{Tref}^{T} Cp_{steam} dT$$

At the outlet of the column the temperature, the flowrate and the concentrations are changing with time, so the enthalpy is calculated as the integral over time of the purge step of:

$$H_{outlet} = \int_{t0}^{tcool} F_{out}\big(y_{CO2}(h_{CO2}(t) - href_{CO2}) + y_{N2}(h_{N2}(t) - href_{N2}) + y_{steam}(h_{steam}(t) - href_{steam})\big)dt$$

For these calculations gases are assumed to be ideal and the heat capacities are taken from Poling et al. (2004). As a simple check to the calculations, assuming that the solid is saturated with the adsorbate at an average temperature of 30 °C, the heat required to heat up the solid to 125 °C and desorb the CO_2 from a single channel will be 125 J, which is close to the enthalpy exchanged during the purge step (137 J for case 3).

Table 5 reports the results for the same configuration for Cases 3 and 4 using steam at 145 °C. The performance is similar but as expected, due to the higher temperature of the steam, less steam is

required but the heat duty remains similar – the increase is due to the higher regeneration temperature.

Table 5. Summary of the parameters used for the case in which the steam used is at 145 °C (only Case 3 and 4 reported).

Parameters	Case 3 (steam @ 145 °C)	Case 4a (steam @ 145 °C)	Case 4b (steam @ 145 °C)
Cycle time, s	1430	1430	1430
Adsorption time, s	72.2	72.2	72.2
F_{feed}, $\frac{m^3/s}{m^2_{mon}}$	2.28	2.28	2.195
F_{purge}, $\frac{m^3/s}{m^2_{mon}}$	1.89	1.89	1.89
F_{N2}, $\frac{m^3/s}{m^2_{mon}}$	1.47	1.47	1.47
Max. Pressure drop, mbar	3.72 (ads) 4.42(cooling)	37.8 (ads) 44.8(cooling)	37.8 (ads) 44.8(cooling)
Max velocity, m/s	5.4 (ads) 4.7(cooling)	5.4 (ads) 4.9(cooling)	5.4 (ads) 4.9(cooling)
Vent time, s	–	1.72	1.72
Vol_{vent}, m^3/ kg CO_2 captured		0.18	0.181
Heat duty, MJ/kg CO_2 captured	5.71	5.7	5.7
Steam required, kg of Steam/kg CO_2 captured	2.87	2.98	2.98
CO_2 Recovery	90	86.8	90
CO_2 Purity	79.9	97	97

The results indicate that while it is possible to meet the pre-set purity and recovery requirements, the consumption of steam is high. This is primarily due to the relatively low CO_2 adsorption capacity of standard activated carbon at a partial pressure of 0.1 bar.

To understand the potential of the process, an additional series of simulations were performed considering the properties of adsorbents which could be developed based on improved materials. A hypothetical next-generation physisorbent and chemisorbent were considered to compare the performance of the process with that obtained using the activated carbon monolith. For a fair comparison it was assumed that the different adsorbents would have the same physical properties of the base monolith (density, void fraction, Cp, etc.) as well as the same N_2 uptake. Figure 5 shows the isotherms for the three adsorbents at 30 and 110 °C; the parameters of the Dual Site Langmuir model are listed in Table 6.

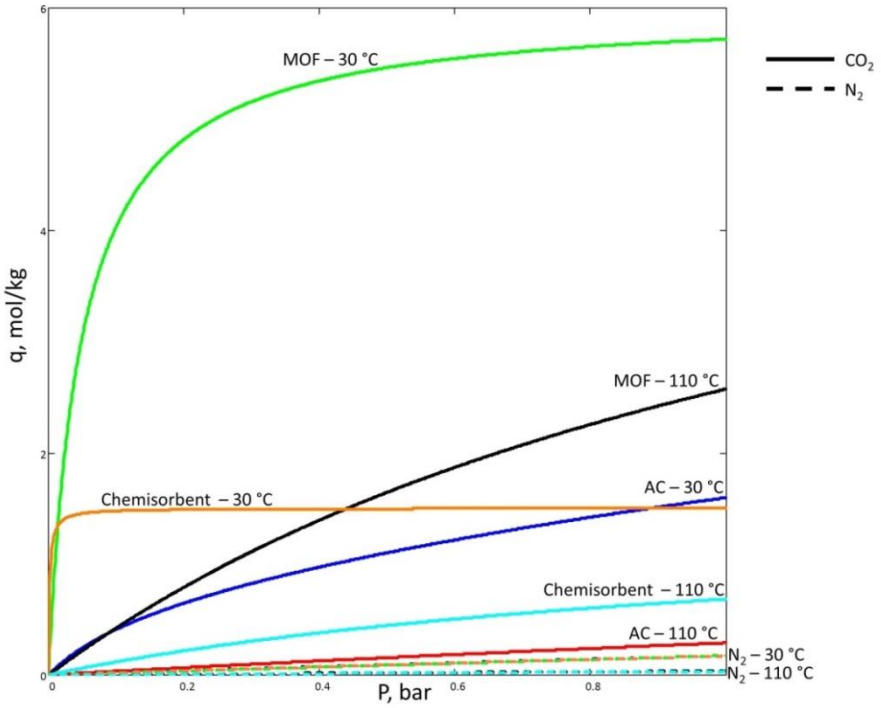

Figure 5: CO_2 and N_2 equilibrium isotherms for the three types of adsorbents considered.

Table 6. Parameters of the Dual Site Langmuir Isotherm for the "hypothetical" MOF and the chemisorbent.

	MOF		**Chemisorbent**	
DSL parameters	**CO_2**	**N_2**	**CO_2**	**N_2**
qs_1, mol/kg	4	4	1	1
qs_1, mol/kg	2	2	0.5	0.5
b_{01}, 1/bar	3×10^{-6}	2.08×10^{-5}	1.23×10^{-11}	1.673×10^{-5}
b_{02}, 1/bar	2×10^{-6}	1.35×10^{-6}	7×10^{-12}	4.61×10^{-5}
ΔH_1, kJ/(mol K)	40	19.3	80	21.87
ΔH_2, kJ/(mol K)	40	18.3	80	20.99

One of the most important features indicating the expected separation performance of any adsorbent is the selectivity of the gas of interest over the other components of the mixture. The limiting ideal selectivity is calculated as the ratio of the Henry's Law Constants for the gas of interest (CO_2, in this case) and the other components of the feed mixture (N_2) and can be used to see the effect of temperature on the selectivity. For the case of the Dual Site Langmuir isotherm this corresponds to:

$$\alpha = \frac{q_{s1}^{CO2} b_1^{CO2} + q_{s2}^{CO2} b_2^{CO2}}{q_{s1}^{N2} b_1^{N2} + q_{s2}^{N2} b_2^{N2}}$$

Figure 6 shows the trend of selectivity with temperature for the three adsorbents. At 30 °C the selectivity for the chemisorbent is about 5000, for the MOF this goes down to 700 while for the activated carbon this value is around 30.

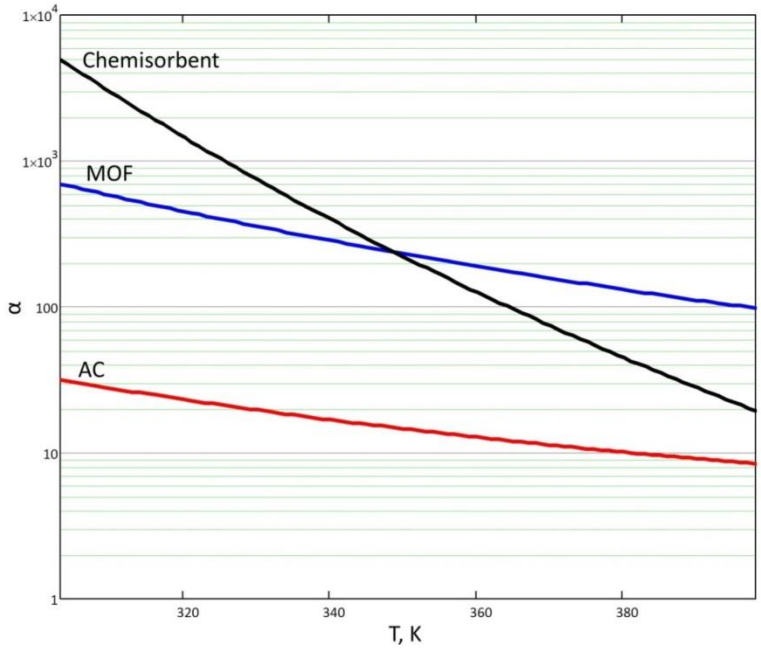

Figure 6: Dependence of the equilibrium ideal selectivity for the three types of adsorbents considered.

M-CPO-27 metal organic frameworks have been tested at the University of Edinburgh as part of US-DoE and EPSRC funded projects. The material with the highest CO_2 capacity is Mg-CPO-27 but it is not stable in the presence of water. Ni-CPO-27 has the second highest CO_2 capacity in the series of materials and is stable. Therefore a hypothetical adsorbent is selected to have the adsorption properties between a Ni-CPO-27 and a Mg-CPO-27. This corresponds to a capacity which is about 30% higher than a commercial 13X zeolite, with a heat of adsorption around 40 kJ/mol.

On the other hand, chemisorbents are generally characterised by lower adsorption capacity (1 to 2 mol/kg at 0.1 bar) and higher heats of adsorption, between 80 and 90 kJ/mol. As a result, isotherms for these materials are almost rectangular with relatively high CO_2 uptake at very low pressures while the high heat of adsorption makes them particularly suitable for temperature swing adsorption processes.

Table 7 shows the performance of Cases 3 and 4 using the “hypothetical” MOF and the chemisorbent. Since the capacity is higher and the flowrates are similar to the previous cases (as these are set by the pressure drop) the cycle time increases. One could reduce the cycle time by reducing the column length, but this was not considered here. The heat of adsorption is higher for these materials and this generates a temperature wave along the column (the maximum temperature rise during adsorption is approximately 50 °C). This results in a similar value of the steam required but the heat duty in desorption is much lower.
For the chemisorbent the lower CO_2 capacity compensates for the higher heat of adsorption, generating a slightly lower temperature rise during the adsorption (about 30 °C). As a result a higher

heat duty is required for the desorption as compared to the MOF, but the amount of steam required is slightly lower.

It can also be noted that the good performance of the two adsorbents allow to achieve almost 97% purity target even without the the N_2 vent step. For this reason a vent of only a fraction of a small second is enough to achieve the pre-set target.

Table 7. Summary of the parameters used for the case in which the adsorbents are "hypothetical" MOF and chemisorbent.

	MOF		**Chemisorbent**	
Parameters	Case 3	Case 4	Case 3	Case 4
Cycle time, s	2090	2090	1969	1969
Adsorption time, s	230.1	230.1	109.08	109.08
F_{feed}, $\frac{m^3/s}{m^2_{mon}}$	1.94	1.94	2.21	2.2
F_{purge}, $\frac{m^3/s}{m^2_{mon}}$	1.71	1.71	1.77	1.77
F_{N2}, $\frac{m^3/s}{m^2_{mon}}$	1.39	1.39	1.39	1.39
Max. Pressure drop, kPa	3.85 (ads) 3.91(cooling)	3.85 (ads) 3.91(cooling)	4.52 (ads) 3.91(cooling)	4.52 (ads) 3.91(cooling)
Max velocity, m/s	4.94 (ads) 4.4(cooling)	4.94 (ads) 4.4(cooling)	4.77 (ads) 4.44(cooling)	4.77 (ads) 4.44(cooling)
Vent time, s	–	0.195	–	0.23
Vol_{vent}, m^3/ kg CO_2 captured		0.012		0.02
Heat duty, MJ/kg CO_2 captured	1.84	1.84	3.38	3.39
Steam required, kg steam/kg CO_2 captured	3.05	3.06	2.77	2.79
CO_2 Recovery	90	90	90	90
CO_2 Purity	95.5	97	94.6	97

Process Performance at Lower CO_2 Concentration

In addition to the cases at a CO_2 concentration of 10%, low concentration cases were also investigated to assess the performance of the process. The three types of adsorbents were compared using the same process configurations as describe above (only cases 3 and 4 were used) but the feed mixture was 4% CO_2 in N_2. Table 8 summaries the key parameters for the process using the different adsorbents. As expected the heat duty increases, but the required purity and recovery are still achieved.

Table 8. Summary of the process parameters for the capture process at 4% CO_2 using the three adsorbents.

	Activated carbon		**Chemisorbent**		**MOF**	
Parameters	Case 3	Case 4	Case 3	Case 4	Case 3	Case 4
Cycle time, s	1480	1480	2088	2088	2270	2270
Adsorption time, s	122.1	122.1	228.4	228.4	410.2	410.2
F_{feed}, $\frac{m^3/s}{m^2_{mon}}$	2.26	2.2	2.21	2.2	1.94	1.93
F_{purge}, $\frac{m^3/s}{m^2_{mon}}$	1.95	1.95	1.8	1.8	1.71	1.71
F_{N2}, $\frac{m^3/s}{m^2_{mon}}$	1.49	1.49	1.39	1.39	1.39	1.39
Max. Pressure drop, kPa	3.62 (ads) 4.19(cooling)	3.51 (ads) 4.18(cooling)	4.33 (ads) 3.91(cooling)	4.33 (ads) 3.91(cooling)	3.63 (ads) 3.91(cooling)	3.63 (ads) 3.91(cooling)
Max velocity, m/s	5.06 (ads) 4.76 (cooling)	5 (ads) 4.76 (cooling)	5.64 (ads) 4.44(cooling)	5.64 (ads) 4.44(cooling)	4.78 (ads) 4.43(cooling)	4.78 (ads) 4.43(cooling)
Vent time, s	–	2.42	–	0.42	–	0.64
Vol_{vent}, m^3/ kg CO_2 captured		0.2		0.034		0.032
Heat duty, MJ/kg CO_2 captured	7.06	7.28	3.97	3.97	2.51	2.52
Steam required, kg steam/kg CO_2 captured	8.04	8.27	7.06	6.97	7.64	7.67
CO_2 Recovery	90	90	90	90	90	90
CO_2 Purity	68.1	97	91.9	97	91.4	97

Tests with Slower Mass Transfer kinetics

As a final comparison it was decided to investigate the effect of the mass transfer kinetics on the performance of the cycle. For this reason a case with a smaller and one with a larger mass transfer coefficient were considered. The conditions chosen are for 10% CO_2 concentration reported in Table 4. The influence of the numerical dispersion was reduced by increasing the grid points from 20 to 50. The time constants was chosen as 10 s^{-1} for the case with fast kinetics and 0.01 s^{-1} for the case with slow kinetics. The time constant for the slow kinetics case was estimated from the kinetics measured by Brandani et al. (2004) on a Mead-Westvaco carbon monolith and includes both the contributions of mass transfer in the solid and dispersion due to the non-homogeneities in the monolith (Ahn and Brandani, 2005b). This represents an extreme case for which the slow kinetics generates a relatively large mass transfer zone along the monolith.

The effect of the results dispersion is significant on the overall performance of the process. In order to achieve the required targets of purity and recovery a large vent step is needed to get rid of the N_2 coming out of the adsorber. The resulting process shows a drop in the productivity of almost 20% as compared to the one in which fast kinetics is assumed.

Table 9. Effect of mass transfer kinetics for the case at 10% CO_2

	τ = 10 s^{-1}		**τ = 0.01 s^{-1}**	
Parameters	Case 3	Case 4	Case 3	Case 4
Cycle time, s	1430	1430	1430	1430
Adsorption time, s	72.2	72.2	72.2	72.2
F_{feed}, $\frac{m^3/s}{m^2_{mon}}$	2.32	2.24	2.24	1.84
F_{purge}, $\frac{m^3/s}{m^2_{mon}}$	1.95	1.95	1.95	1.95
F_{N2}, $\frac{m^3/s}{m^2_{mon}}$	1.39	1.39	1.39	1.39
Max. Pressure drop, kPa	3.9 (ads) 4.02(cooling)	3.8 (ads) 4.02(cooling)	3.7 (ads) 4.02(cooling)	3.9 (ads) 4.02(cooling)
Max velocity, m/s	5.3 (ads) 4.44(cooling)	5.2 (ads) 4.44(cooling)	5.2 (ads) 4.44(cooling)	5.3 (ads) 4.44(cooling)
Vent time, s	–	1.54	–	18.6
Vol_{vent}, m^3/ kg CO_2 captured		0.132		1.314
Heat duty, MJ/kg CO_2 captured	4.85	4.95	4.96	6.03
Steam required, kg of steam/kg CO_2 captured	2.95	3.01	3.01	3.67
CO_2 Recovery	90	90	90	90
CO_2 Purity	80	97	78.7	97

Conclusions

The performance of the separation process based on the use of a monolith in a rotary wheel system was analysed considering cases with different CO_2 concentrations, different steam temperatures and different adsorbents. Using a carbon monolith the pre-set targets of CO_2 recovery and purity can be achieved, but a relatively high heat duty/steam consumption is required in the desorption step. This is mainly due to the relatively low capacity of the adsorbent chosen for the separation.
The process becomes significantly more competitive if an improved adsorbent is used, such as a highly performing physisorbent or chemisorbent. From the comparison of the three adsorbents, the "hypothetical" MOF resulted to be the best choice for the process both at the higher and lower CO_2 concentration, with less than 2 MJ/kg of CO_2 captured required for the separation at 10 % CO_2. The chemisorbent on the other hand, thanks to the shape of the isotherm, provided similar performances at high and low CO_2 concentration and the adsorption capacity is not affected by the presence of water.
The case with the slow kinetics shows that the effect of the mass transfer zone needs to be minimised since it will have a significant effect on the overall performance of the process. This, combined with the considerations on the effect of the equilibrium properties of the adsorbent, suggests that in order to have a competitive separation process a careful optimisation of the adsorbent material and monolith configuration is required.
The original question posed to us was to determine if the process could deliver 90% purity and 97% recovery. The simulations have shown that an ideal system can be configured to achieve these targets, and the inclusion of a short vent step helps in meeting the requirement of 97% purity.

References

Agueda V.I., Crittenden B.D., Delgado J.A., Tennison S.R. Effect of Channel Geometry, Degree of Activation, Relative Humidity and Temperature on the Performance of Binderless Activated Carbon Monoliths in the Removal of Dichloromethane from Air. *Separation and Purification Technology*, 2011, 78, 154–163.

Ahn H. and Brandani S. Analysis of Breakthrough Dynamics in Rectangular Channels of Arbitrary Aspect Ratio, *AIChE J.*, 2005a, 51, 1980–1990.

Ahn H. and Brandani S. Dynamics of Carbon Dioxide Breakthrough in a Carbon Monolith Over a Wide Concentration Range, *Adsorption*, 2005b, 11, 473–477.

Brandani F., Rouse A., Brandani S. and Ruthven D.M. Adsorption Kinetics and Dynamic Behavior of a Carbon Monolith, *Adsorption*, 2004, 10, 99–109.

Cornish R.J. Flow in a Pipe of Rectangular Cross-Section, *Proc. R. Soc.*, 1928, 120, 691–700.

Poling B.E., Prausnitz J.M., O'Connell J.P. *The Properties of Gases and Liquids*. Fifth Edition. McGraw-Hill. New York. 2004.